applied sciences

MDPI

Article

Numerical Analysis of the Overtopping Failure of the Tailings Dam Model Based on Inception Similarity Optimization

Deli Qiu [1], Jiangdong Xu [2] and Hai Lin [2,*]

[1] Jiangxi Provincial Architectural Design and Research Institute Group Co., Ltd., Nanchang 330046, China; jxjskc@126.com
[2] School of Infrastructure Engineering, Nanchang University, Nanchang 330031, China; xd13399@outlook.com
* Correspondence: linhai@ncu.edu.cn

Abstract: The analysis of overtopping dam break caused by extreme rainstorms and other special circumstances is very important in the feasibility analysis of new construction or expansion projects of tailings reservoirs. Reduced-scale physical model tests can directly reflect the topography and dam-break influence range, but the reasonable selection of model dam material is the key to ensure the model's similarity. Based on the similarity optimization of the limit state of scour inception of sediment particles, a new method for the model material of tailings dams can be proposed, but it needs to be verified by a similar overtopping model test. In this paper, the modeling and numerical calculation analysis of a prototype tailings dam and a similar reduced-scale model are carried out by using FLOW-3D v11.2 numerical software. The calculation results show that the model test scheme optimized by inception similarity can well reproduce the overtopping failure process of the prototype dam.

Keywords: tailings dam; overtopping failure; inception similarity; numerical analysis

Citation: Qiu, D.; Xu, J.; Lin, H. Numerical Analysis of the Overtopping Failure of the Tailings Dam Model Based on Inception Similarity Optimization. *Appl. Sci.* **2024**, *14*, 990. https://doi.org/10.3390/app14030990

Academic Editor: Tiago Miranda

Received: 29 November 2023
Revised: 15 January 2024
Accepted: 20 January 2024
Published: 24 January 2024

1. Introduction

The high-energy debris flow generated after tailings dam failure poses a major safety threat to downstream residents and facilities, and tailings dam failure will cause serious environmental pollution [1–5]. Among the main causes of tailings dam failure, overtopping dam break is difficult to prevent [6]. Extreme climate combined with the failure of spillway and other drainage facilities will lead to the rapid rise of reservoir water levels and overtopping, and the corresponding risk assessment and emergency operation response are important links in the feasibility analysis of related projects [7,8]. Under the action of overtopping flow, the tailings dam will be eroded and gradually develop into dam failure [9–11]. Due to the unpredictability of extreme climate and other influencing factors, it is necessary to analyze the impact of overtopping failure on newly built or expanded tailings reservoirs [12].

In engineering practice, two main methods are usually used to analyze the influence of overtopping dam break on the downstream, which are physical model tests and numerical modeling calculation. The reduced-scale physical model test method is intuitive and can consider the complex spatial characteristics of the site, which has certain advantages in the project decision analysis. Good similarity between overtopping dam-break model and prototype is the premise of the physical model test, and reasonable selection of tailings dam model material is the key to ensure the similarity of the tailings dam-break process [13]. In practice, the dam overtopping model test often uses the same soil or even the same compaction state as the prototype. The previous studies of the cohesion of sediment particles shows that the selection of the model scale of overtopping dam failure may affect or change the movement form of sediment in the process of breaking, so it is recommended to use a large-scale ratio as far as possible to design the model [14–16]. In the normal gravity physical model test of cohesionless soil, the use of model sand with small internal friction angle can improve the similarity between the mechanical properties of the material and the prototype, but it is very difficult to achieve complete similarity [17].

In the overtopping model test, the scouring process of the reduced-scale model must be similar to that of the prototype, so the similarity of the model sand is an important criterion for the model design [18]. The similarity of sediment incipient motion under the action of gravity flow is an important condition for determining the simulated sand, so the analysis of sediment incipient motion state is the key to the similarity analysis of the overtopping dam-break model. However, due to the complexity of the real environment of the riverbed, the stress of different tailings particles may be different because of the geometric shape, size, volume, weight and other factors. It is quite challenging to simulate the incipient state under the action of similar water flows in model tests. In the study by Lin [18], recommendations were given for the selection of tailings dam materials in model tests based on the similarity analysis of the critical incipient state of the material. Furthermore, the optimization of the inception similarity was validated through chute inception tests. In order to better explore the model test technology of tailings dam break due to overtopping flow, this paper designs and carries out the numerical test of a prototype and model based on the principle of inception similarity optimization, and the results further show that inception similarity optimization can make the test technology of tailings dam break closer to prototype reality.

2. Inception Similarity Optimization Analysis

The movement modes of sediment under the action of shear flow are divided into three types: suspension, jumping and transport [19,20]. The transport of sediment refers to the sliding and rolling of sediment particles along the bottom of the riverbed. The phenomenon of sediment transport has little to do with the type of flow. The formation of the sediment transport phenomenon is due to the coaction of the drag force generated by the shear flow and the internal frictional resistance of sediment. At the same time, the uplift force of the shear flow is not enough to make the sediment suspend. The transport motion of sediment is the most common movement mode besides suspension. Taking the critical incipient state of the tailings on the dam surface as the research object, similarity analysis was conducted for the overtopping dam in transport mode. Based on the inception similarity analysis in Lin et al. [18], tailings particles can achieve force equilibrium in both the horizontal and vertical directions at the critical condition of inception (Figure 1), assuming that tailings particles are spherical in shape. The drag force due to the waterflow F_D, resistance F_f, uplift force F_L and underwater gravity W can be represented as follows:

$$F_D = C_D \frac{\pi d^2}{4} \frac{\rho u_b^2}{2} \tag{1}$$

$$F_f = \tau_f A_f = \tau_f \frac{\pi d^2}{4} \tag{2}$$

$$W = \frac{\pi}{6} (\gamma_s - \gamma) d^3 \tag{3}$$

$$F_L = C_L \frac{\pi d^2}{4} \frac{\rho u_b^2}{2} \tag{4}$$

where C_D is the drag coefficient of waterflow; C_L is the uplift coefficient; d is the diameter of sediment particles (m); ρ is the density of waterflow (kg/m^3); u_b is the instantaneous velocity of waterflow acting on the surface of bedload particles (m/s); τ_f is the shear strength of mud bed (Pa); A_f is the area of particles (m^2); γ_s is the bulk density of sediment (kg/m^3); γ is the bulk density of waterflow (N/m^3).

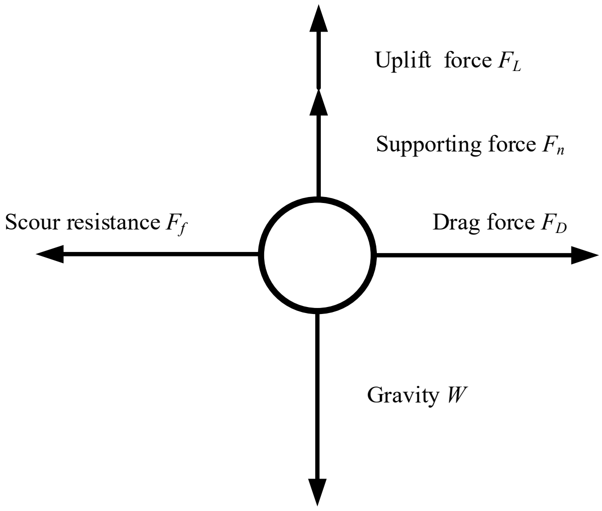

Figure 1. Schematic diagram depicting the force analysis for initiating sediment particle movement.

It can be seen from the sediment movement mechanics and the turbulent inception test that the shear stress of the flow on the riverbed sediment is related to the Reynolds number [21]. The actual flow in the process of overtopping dam break of the tailings pond is mainly turbulent flow; that is, the Reynolds number is very large. The surface flow velocity of sediment particles reaching mechanical equilibrium and just initiating motion under turbulent flow conditions (also known as the critical shear velocity) can reflect the magnitude of bed shear stress in open channel flow. The horizontal drag force exerted on sediment particles by water flow can be expressed as:

$$\tau_{cr} = \rho u_b^2 \tag{5}$$

where τ_{cr} is the critical inception shear resistance.

In the horizontal force direction of sediment particles, the equilibrium equation is established:

$$F_D = F_f \tag{6}$$

The relationship between critical shear stress and sediment surface velocity can be derived from Equations (1), (3) and (6):

$$u_b^2 = \frac{2\tau_{cr}}{C_D \rho} \tag{7}$$

An equilibrium equation is established in the vertical stress direction of the sediment particles:

$$F_n = W - F_L \tag{8}$$

According to the soil mechanics mentioned, considering the non-viscosity between the particles, the expression of shear strength can be obtained:

$$\tau_f = \sigma_n \cdot tan\phi \tag{9}$$

where τ_f is the shear strength (Pa); σ_n is the stress acting on sediment particles (Pa); ϕ is the Internal friction angle of sediment (rad/°).

The normal stress of tailings particles acting on the subsoil can be expressed by the supporting force:

$$\sigma_n = \frac{F_n}{A} = \frac{W - F_L}{\frac{\pi d^2}{4}} \tag{10}$$

Substituting Equations (8) and (10) into Formula (9), it can be seen that the initial shear stress of tailings particles can be related to the gravity, drag force and shear strength of tailings:

$$\tau_f = \frac{W - F_L}{\frac{\pi d^2}{4}} \tan \phi \quad (11)$$

Substituting Formulas (5) and (7) into (11) for conversion, the following relationship can be obtained among the internal friction angle, particle size and incipient shear stress of sediment:

$$\tan \phi = \frac{\tau_{cr}}{\frac{2}{3}(\gamma_s - \gamma)d - C_L \frac{\tau_{cr}}{C_D}} \quad (12)$$

Equation (12) can be transformed to obtain the relationship between the incipient shear stress of sediment particles and the mechanical parameters of rock and soil materials:

$$\tau = \frac{\frac{2}{3}(\gamma_s - \gamma_w)d_{50} tan\varphi}{1 + \alpha tan\varphi} \quad (13)$$

The incipient shear stress can be obtained from the hydraulic parameters at the incipient moment [22]:

$$\tau = \frac{\gamma}{g}u_*^2 = \frac{\gamma}{g}\left(\frac{u_L}{A + 5.75 log\frac{L}{d}}\right) \quad (14)$$

In the formula, the recommended value of the coefficient A is 8.48 [22]; L is the water depth (m); u_* is the friction velocity (m/s); d is the particle size of sediment particles (m); and u_L is the flow velocity corresponding to the water depth of sediment particles at the bed surface (m/s). The classical Formula (14) is simple and practical. Although it has some shortcomings in dimensional analysis, it is an empirical formula verified by a large number of tests. According to the similarity of sediment incipient shear stress, the selection or adjustment method of model sand can be found, which makes the relevant preparatory tests more targeted.

3. Numerical Test Method and Scheme Design

Numerical Calculation Method

In order to verify the similarity of the model overtopping process by selecting the model tailings dam material with optimized incipient velocity, numerical tests were carried out taking a tailings dam in southern China as prototype. The FLOW-3D software is used for modeling and analysis of the numerical experiment. According to the design scheme of the prototype tailings dam, the prototype tailings dam is 26 m high and 770 m long. The downstream slope ratio of the dam is about 1:5, and the slope ratio inside the tailings pond is about 1:100 (Figure 2). A small opening is made at the top of the dam to predetermine the point of overtopping. When overtopping occurs, the overtopping water flow scours the tailings dam continuously under the action of gravity, and the tailings on the dam body begins to start and move together with the waterflow when the overtopping flow reaches a certain velocity. To better observe the dam-break process and better judge the discharge of tailings as well as the change of upstream water level, the upstream and downstream areas of the dam should be included in the establishment of the numerical model.

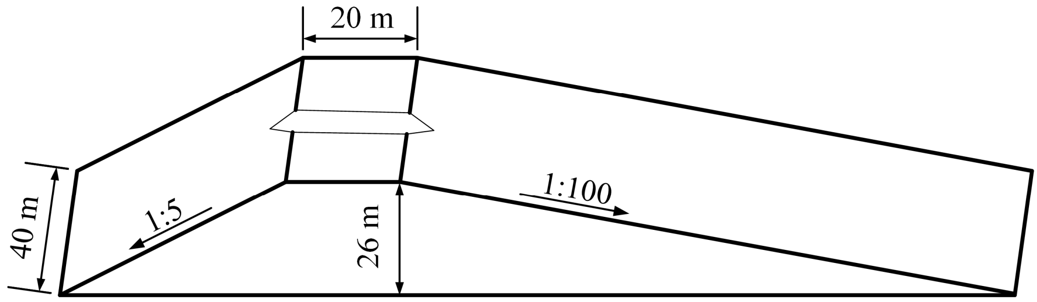

Figure 2. Schematic diagram of the prototype tailings dam.

According to the actual size of the prototype tailings dam and in combination with the scale of the indoor model test, the width of 40 m of the prototype tailings dam is intercepted for numerical testing to observe the dam-break characteristics of the prototype tailings pond. Therefore, a prototype analysis area with a value range of 260 m × 40 m × 26 m is established (Figure 3). When considering the overtopping, the water head height in the reservoir should be greater than the elevation of the dam crest, and the inflow can be added to the calculation area by setting the pressure boundary. However, considering the pressure boundary condition, the inflow water has a certain initial water pressure, which will produce a certain initial pressure on the reservoir water, resulting in too fast fluid velocity when the dam fails, and the dam scour is quite different from the actual situation. In order to solve the influence of the initial pressure caused by the pressure boundary on the experimental results, a baffle is set behind the water area in the reservoir to block the pressurized water. After the water overflows the baffle, it flows into the water area in the reservoir. At this time, the initial pressure caused by the pressure boundary is effectively buffered. Therefore, it can well simulate the water level rise in the reservoir caused by precipitation and mountain torrents, and the overtopping dam break due to the water body under the action of gravity.

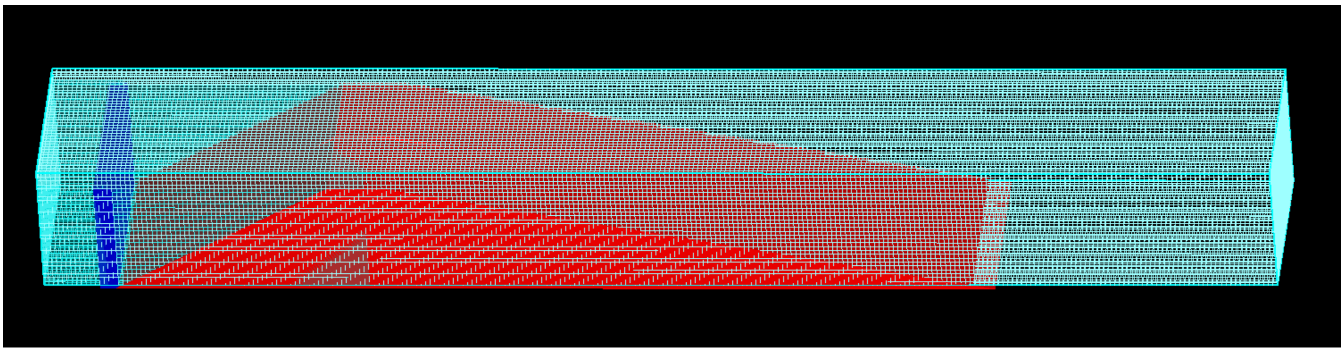

Figure 3. Dam-break calculation model and mesh division.

To achieve better calculation convergence, the grid of this model is selected to be equal in length, width and height; that is, the calculation element is set as a cube element. FAVOR is a method that incorporates geometric effects into the governing equations [23]. The FAVOR technique uses the solid volume fraction in each grid to determine the surface of the solid, establish the control fluid and make the grid geometry completely independent (Figure 4). Using FAVOR technology in dam-break simulation, the sediment volume fraction parameters in the grid can be calculated accurately, so that the form and state of dam failure can be described accurately. In the numerical simulation, the sediment is controlled by the equation of motion. The purpose of dividing the grid is to discretize the relevant area of tailings dam break, so that the motion equation can be calculated and solved on the discretized grid. Compared with the traditional mesh processing technology, FAVOR shows higher efficiency of the operation. The mesh processed by the FAVOR method not only simulates the solid boundary well but also uses fewer meshes, which would greatly improve the efficiency of the operation. After several times of calculation trials and comparison of the influence of the number of grids on the calculation results, it is finally determined that the formal analysis is conducted while the number of grids lies between 300,000 and 500,000 (Figure 3).

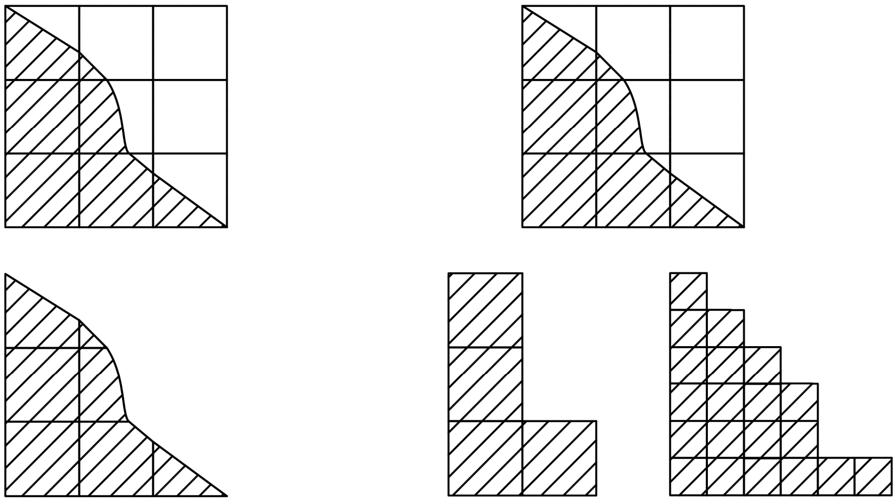

Figure 4. On the left is the geometry depicted using the FAVOR method, and on the right is the geometry depicted using the traditional FDM method.

A numerical calculation model of the indoor launder overflow dam failure test was established with a similar scale of 1:100 between the prototype of the planned tailings dam and the proposed reduced-scale model. Referring to the model tailings selection method recommended by Lin et al. (2023) [18], the dam failure analysis of the reduced-scale model test was analyzed under three schemes: fly ash mixed with bentonite (4:1), fine-grained tailings and prototype tailings, respectively, and the similarity between the model and the prototype and the rationality of the sand selection scheme were verified by combining the characteristics of the dam failure, such as the change of the breach and the time of the dam failure. According to the gravity similarity law, the geometric parameters of the numerical test are designed as shown in Table 1.

Table 1. Design of numerical test parameters.

Program	Height and Width of Dam Body H × W (m)	Slope Ratio	Computational Domain L × W × D (m)	Flow Head (m)
Tailings dam prototype	40 × 26	1:5	260 × 40 × 26	0.5
Fly ash mixed with bentonite (4:1)	0.4 × 0.26	1:5	2.6 × 0.4 × 0.26	0.005
Fine tailings	0.4 × 0.26	1:5	2.6 × 0.4 × 0.26	0.005
Prototype tailings	0.4 × 0.26	1:5	2.6 × 0.4 × 0.26	0.005

Gravity model, sediment scouring model and RNG turbulence model are selected in the numerical simulation, and the physical and mechanical properties of the model packed sand are defined by the tailings particle size, density, critical shields parameter, entrainment coefficient, bed load transport rate coefficient and angle of repose underwater, respectively. The particle size distribution and density of tailings sand can be determined by standard tests (according to ASTM D6913M-17 and ASTM D854-23 [24,25]). In order to achieve a more ideal calculation result, considering the large span of the particle size of the tailings, the average particle size of each particle size range is taken according to the grading curve of the tailings. The critical shields parameter is obtained from the Soulsby & Whitehouse equation. The angle of repose under water is approximated to that of the internal friction angle of tailings. Considering the difference of copper tailings and ordinary sediment properties, the entrainment coefficient is 0.003, which can achieve good test results. According to the physical and mechanical test of rock and soil and the grain grading curve, the sand content of each grain size in the tailings can be obtained, and the purpose of adjusting the reasonable grain grading of the sand can be achieved by setting the percentage content in the model setting. According to the principle of similarity, the physical and mechanical properties of the prototype tailings and the tailings used in the model are listed in Tables 2–4.

Table 2. Properties of prototype tailings.

Name	Average Particle Size (mm)	Density (kg/m^3)	Critical Shields Parameter	Entrainment Coefficient	Bed Load Transport Rate Coefficient	Angle of Repose Underwater
<0.01 mm	0.005	2970	0.3	0.003	8	28.7°
0.01–0.074 mm	0.04	2970	0.29	0.003	8	34.7°
0.074–0.25 mm	0.12	2970	0.28	0.003	8	34.7°
0.25–0.5 mm	0.37	2970	0.26	0.003	8	34.7°

Table 3. Properties of fly ash mixed with bentonite (4:1).

Name	Average Particle Size (mm)	Density (kg/m^3)	Critical Shields Parameter	Entrainment Coefficient	Bed Load Transport Rate Coefficient	Angle of Repose Underwater
<0.005 mm	0.003	2170	0.3	0.003	8	24.3°
0.005–0.01 mm	0.008	2170	0.3	0.003	8	24.3°
0.01–0.05 mm	0.03	2170	0.3	0.003	8	24.3°
0.05–0.1 mm	0.07	2170	0.3	0.003	8	24.3°
0.1–0.5 mm	0.3	2170	0.3	0.003	8	24.3°

Table 4. Properties of fine tailings mixed with 5% fly ash.

Name	Average Particle Size (mm)	Density (kg/m^3)	Critical Shields Parameter	Entrainment Coefficient	Bed Load Transport Rate Coefficient	Angle of Repose Underwater
<0.005 mm	0.003	2970	0.3	0.003	8	28.7°
0.005–0.01 mm	0.007	2970	0.3	0.003	8	28.7°
0.01–0.03 mm	0.02	2970	0.3	0.003	8	34.7°
0.03–0.05 mm	0.04	2970	0.29	0.003	8	34.7°

Based on the relevant engineering data of the tailings pond, the initial condition settings primarily include the global pressure, water pressure calculation method, and the setting of upstream and downstream water levels. The water level in the tailings pond is set at the same elevation as the dam height, which is 26 m. In the model, the bottom is set as a rigid body wall boundary, while the sides are set as symmetric boundaries. The inflow edge and the upper surface are set as pressure boundaries, allowing for either a fixed or time-dependent water head. The rear boundary of the model is a liquid water head outflow boundary, which means that fluid can flow out from and back into this boundary.

4. Test Results

4.1. Prototype Breach Development Process

In the numerical simulation of the prototype tailings dam, the shape deformation of the dam crest section at the beginning of overtopping, 10 min after overtopping, 30 min after overtopping, 50 min after overtopping, 80 min after overtopping and 100 min after overtopping are shown in Figure 5. At the beginning of overtopping, the flow begins to flow out along the pre-opened small gap, and the sediment on the dam crest shows a certain suspension property. Under the entrainment of the flow, the surface of the dam crest is uneven. After 10 min of overtopping, the breach develops slightly, and the downstream of the dam slope is scoured along the slope in a Y shape under the scouring of the water flow. After 30 min of overtopping, slight scouring damage occurs at the dam toe, and a small amount of sediment is deposited at the dam toe. After 50 min of overtopping, the breach developed obviously, the width and depth increased further, and the breach began to form at the toe of the slope. After 80 min of overtopping, the breach at the foot of the slope develops and continues to develop to the top of the dam, and the "deep ditch" formed by water scouring deepens and widens continuously. At this time, the breach at the top of the dam does not develop much. After 100 min of overtopping, a connected breach was formed from the toe of the slope to the top of the slope, and the dam was almost completely destroyed.

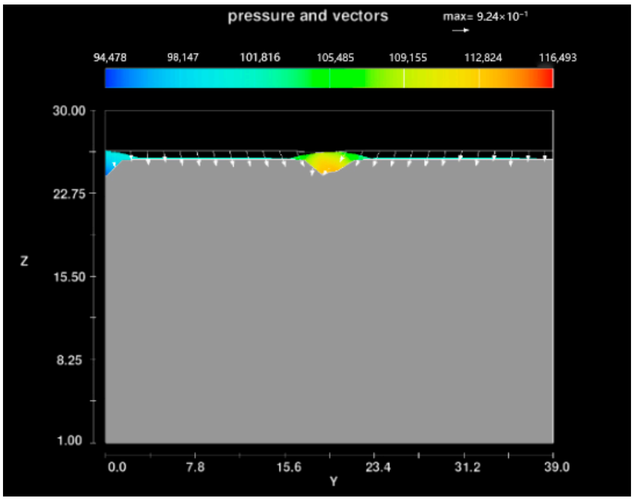

(**a**) Start of overtopping

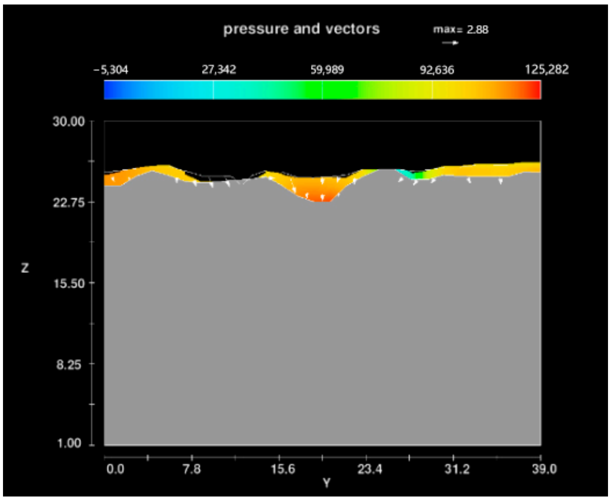

(**b**) 10 min after overtopping

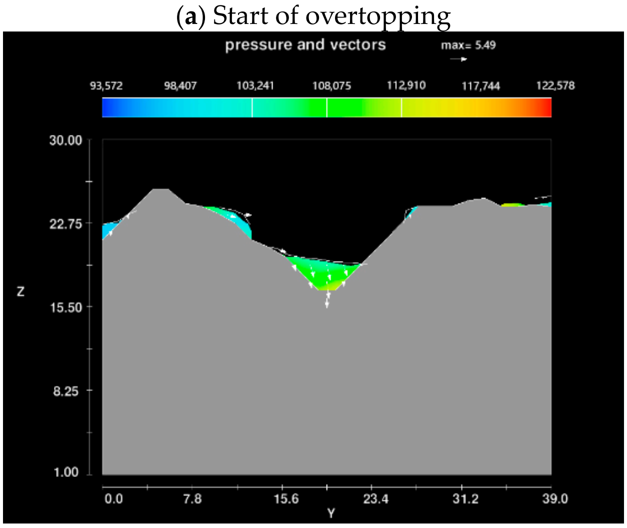

(**c**) 30 min after overtopping

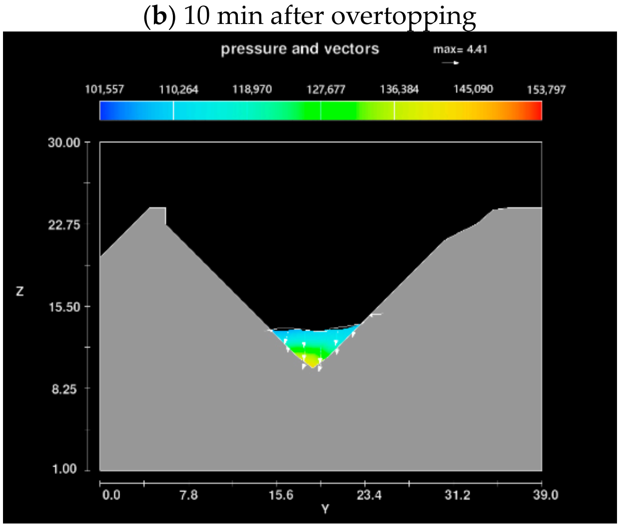

(**d**) 50 min after overtopping

Figure 5. *Cont.*

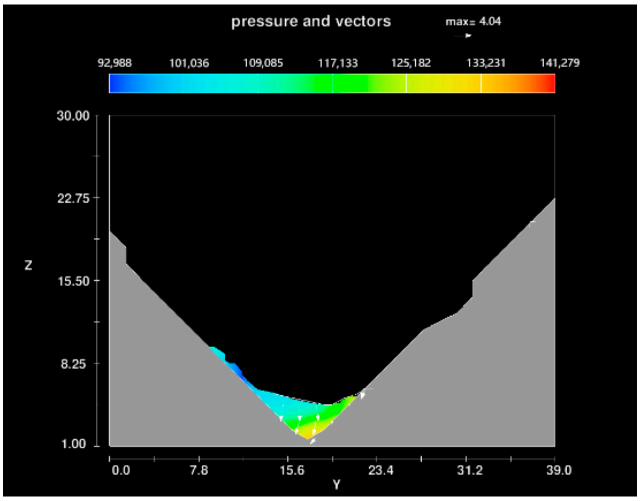

(**e**) 80 min after overtopping

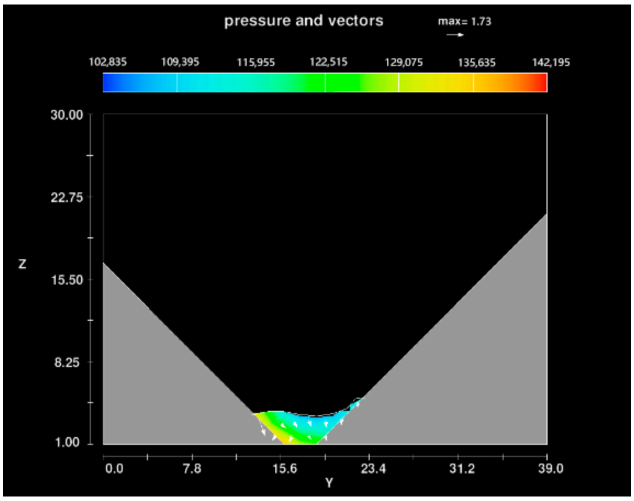

(**f**) 100 min after overtopping

Figure 5. Development of breach of tailings dam.

4.2. Characteristics of Overtopping Dam Break

As the water level rises, the water flow begins to overflow the top. The water flow first flows out along the pre-opened small gap (Figure 6a). With the flow of the water body, the sediment is continuously entrained and scoured. When the dam is overtopped for 10 min, a Y-shaped area is formed at the downstream side of the dam slope (Figure 6b). The distribution of waterflow on the surface of the dam body is relatively uniform at this moment. As the erosion by the water flow proceeds, the erosion the dam surface with the concentrated water flow is accelerated while forming several concentrated channels. As the water flow continues to scour, the channels expand and gradually connect to form a deeper trench (i.e., breach) through the slope of the dam body (Figure 6c). Under the action of waterflow, the sediment on both sides of the trench can be scoured continuously. The width of the breach develops under the action of gravity. The sediment at the bottom of the trench is also scoured continuously, and the breach develops to the deep part (Figure 6e,f). Due to the undercutting effect of the water flow, the scarp damage form will appear locally. As the waterflow carries sediment away, it is often difficult to keep the flow straight because of tailings sedimentation. As the breach develops continuously with time, the section of the deep trench expands continuously until the dam body is destroyed.

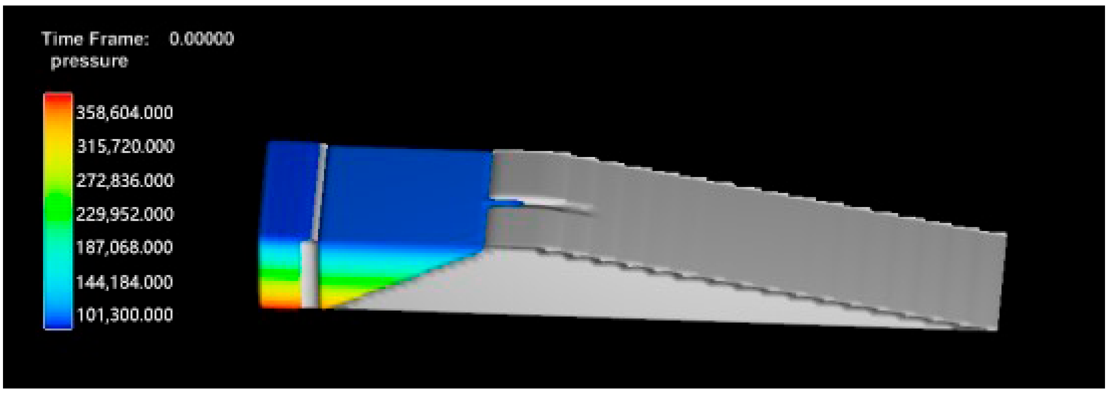

(**a**) Start of overtopping

Figure 6. *Cont.*

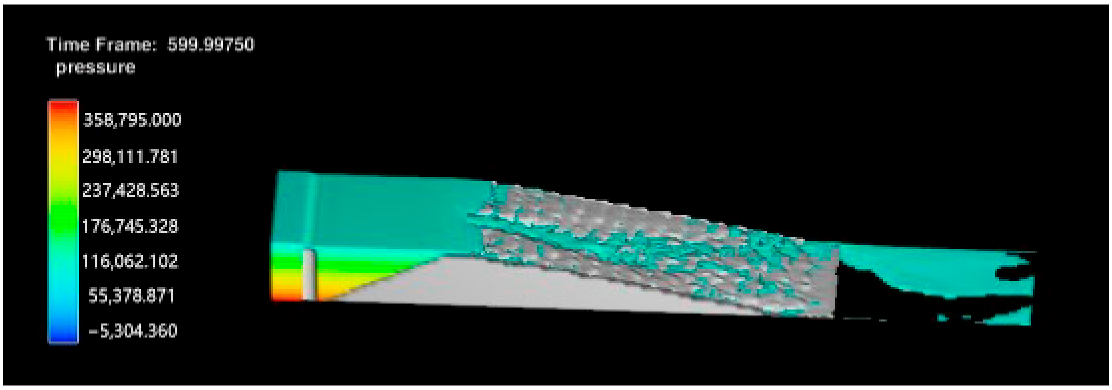

(**b**) 10 min after overtopping

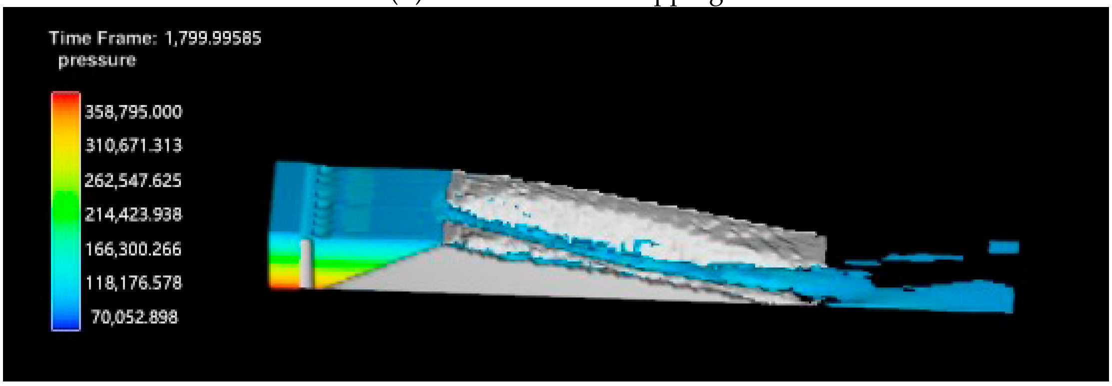

(**c**) 30 min after overtopping

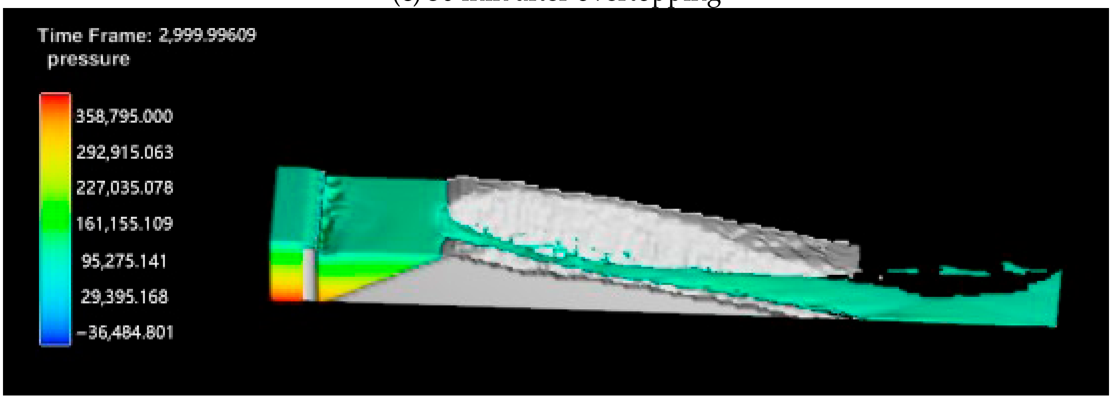

(**d**) 50 min after overtopping

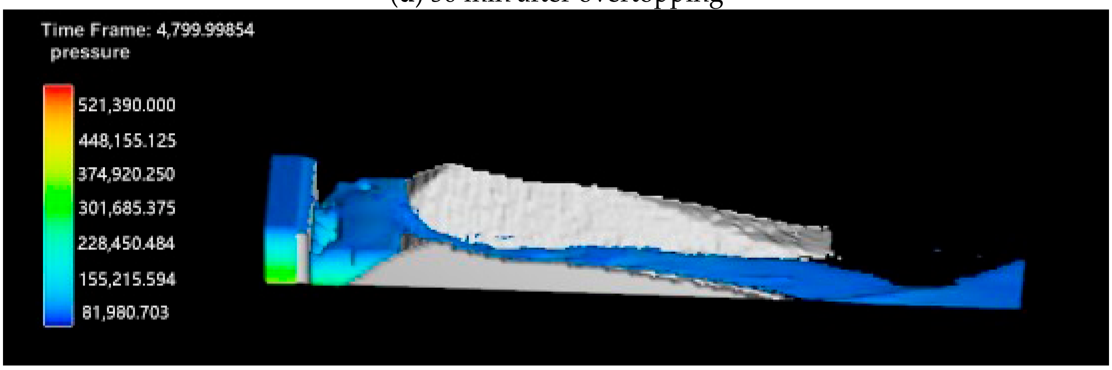

(**e**) 80 min after overtopping

Figure 6. *Cont.*

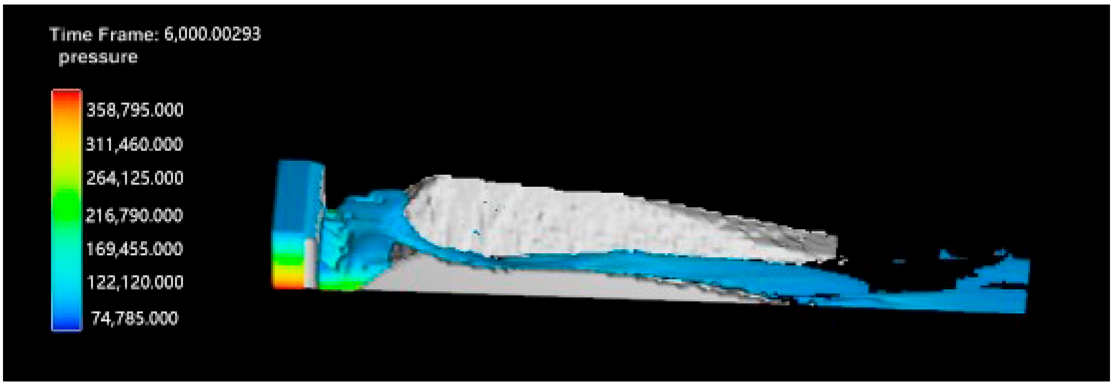

(**f**) 100 min after overtopping

Figure 6. Breakage process of prototype tailings dam.

5. Overtopping Dam-Break Characteristics of Reduced-Scale Models

5.1. Fly Ash Mixed with Bentonite (4:1) Scheme

In the scheme of fly ash mixed with bentonite (4:1), the breach shapes of the model dam crest section at the beginning of overtopping, 1 min after overtopping, 3 min after overtopping, 5 min after overtopping, 8 min after overtopping and 10 min after overtopping are shown in the Figure 7. According to the numerical simulation results, at the beginning of overtopping, the dam crest interface is relatively flat, and the flow at the pre-opened small gap is relatively concentrated. About one minute after overtopping, the dam crest interface becomes uneven. Due to the fine particles of fly ash, the sediment shows certain suspension characteristics. At this time, the grooves formed on the surface of the dam due to the scouring of water flow are obvious. About 3 min after overtopping, the breach develops rapidly, its width increases and the depth deepens to 0.1 m. The flow of water scoured the trench further, and sediment deposits began to appear at the dam toe. About 5 min after overtopping, the width of the breach is further increased, and the depth is further deepened to 0.2 m. The breach develops downstream of the dam slope, and a large amount of sediment is deposited at the dam toe. About 8 min after overtopping, the breach width reaches the maximum, and the breach depth changes little. Meanwhile, the downstream breach of the dam slope is formed, and the downstream sediment is continuously scoured (as shown in Figure 8). The breach continues to develop towards the crest of the dam. After 10 min of overtopping, the depth of the breach reached the maximum, and the dam body was almost completely washed out.

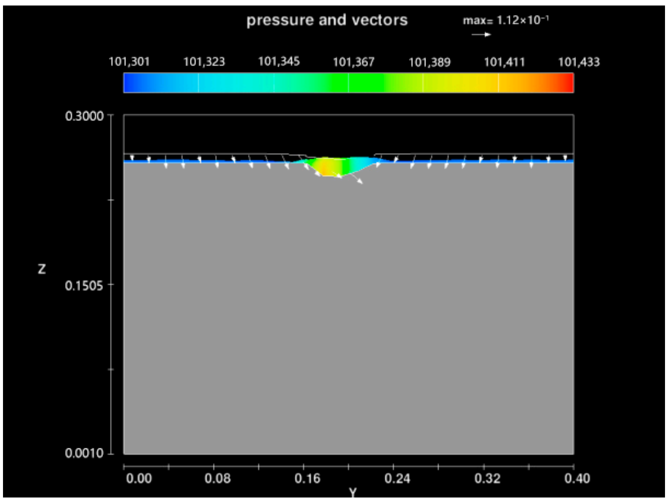

(**a**) Start of overtopping

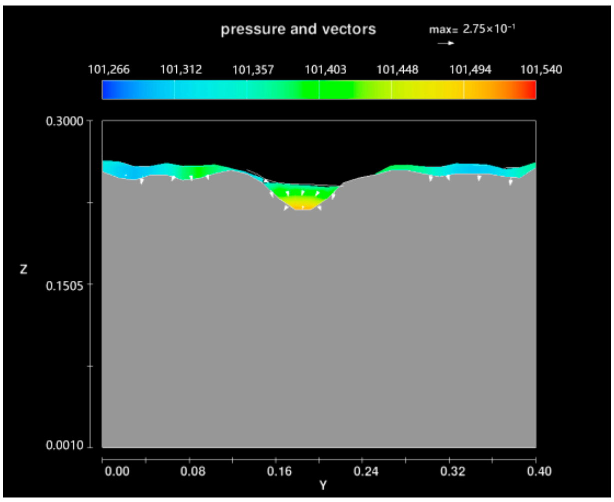

(**b**) 1 min after overtopping

Figure 7. *Cont.*

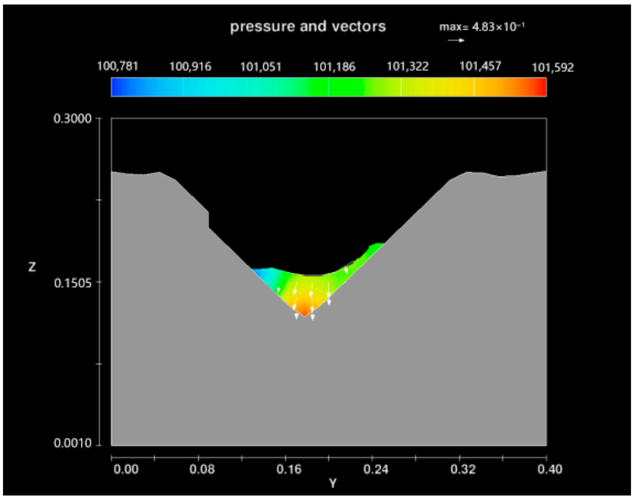

(**c**) 3 min after overtopping

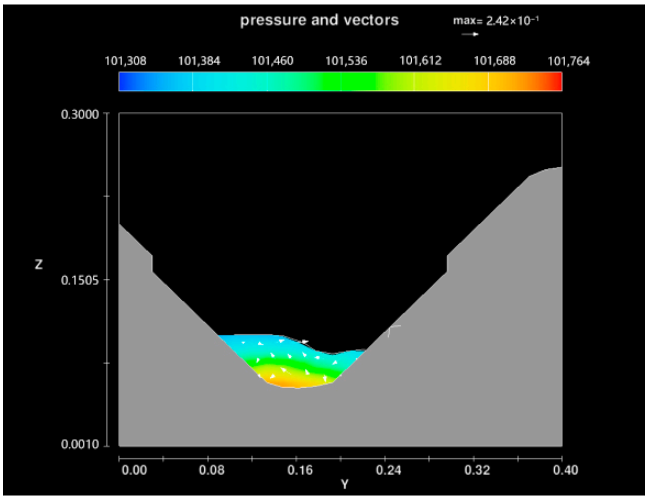

(**d**) 5 min after overtopping

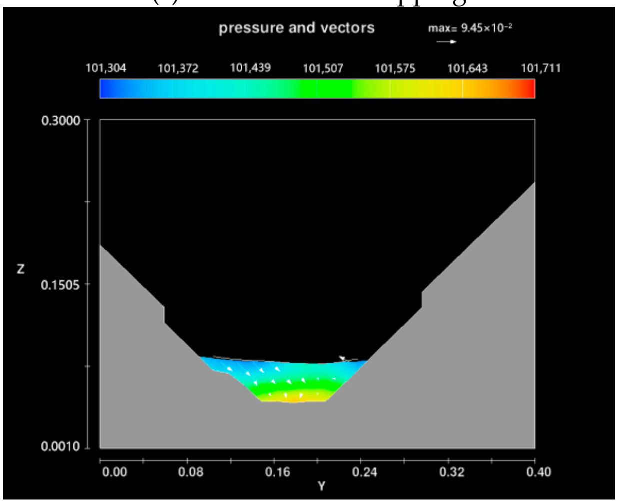

(**e**) 8 min after overtopping

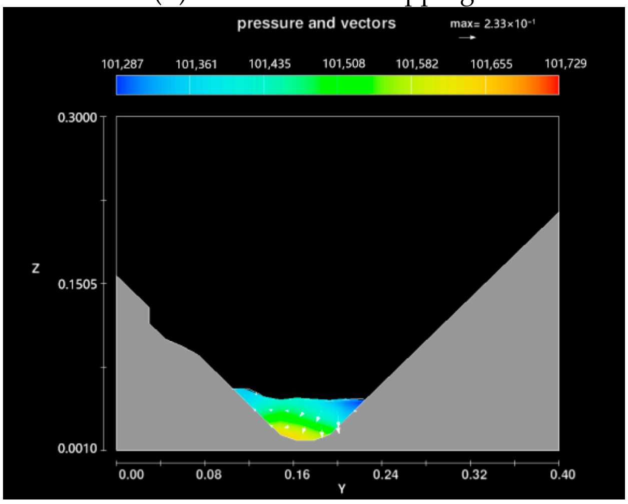

(**f**) 10 min after overtopping

Figure 7. Burst development of fly ash mixed with bentonite (4:1) scheme.

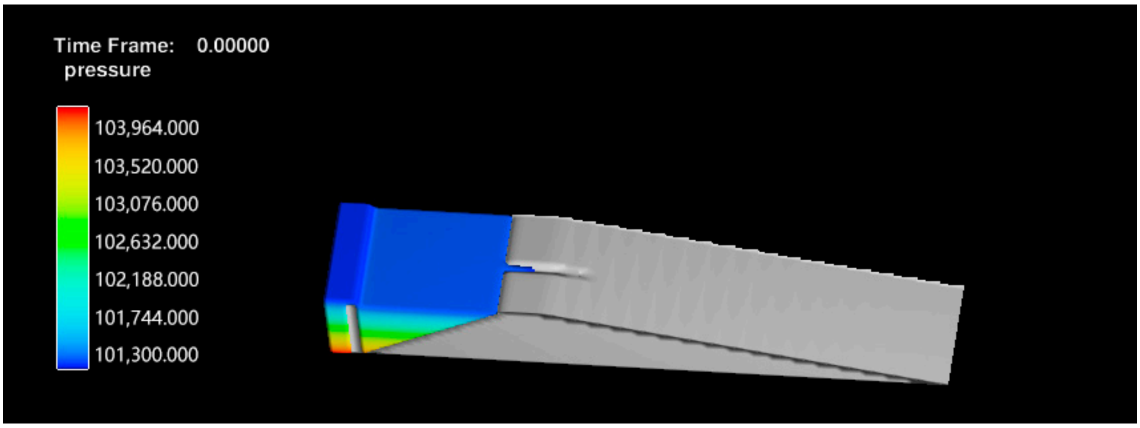

(**a**) Start of overtopping

Figure 8. *Cont.*

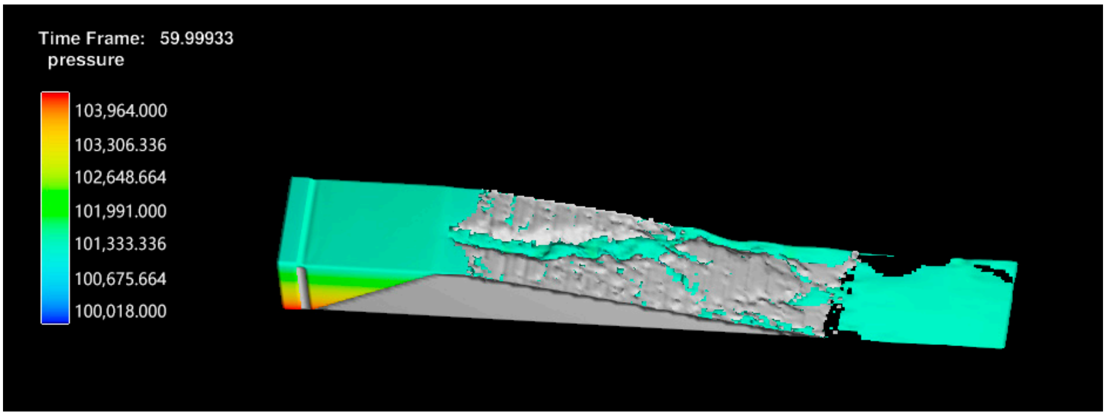

(**b**) 1 min after overtopping

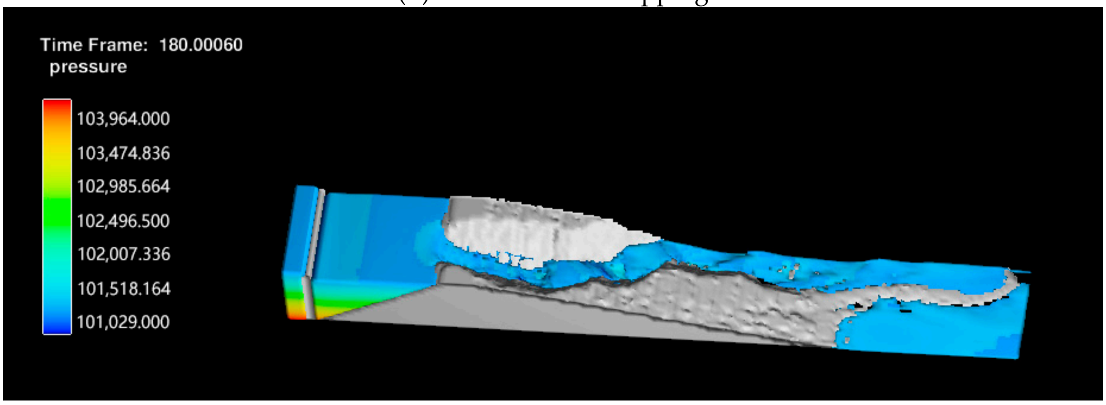

(**c**) 3 min after overtopping

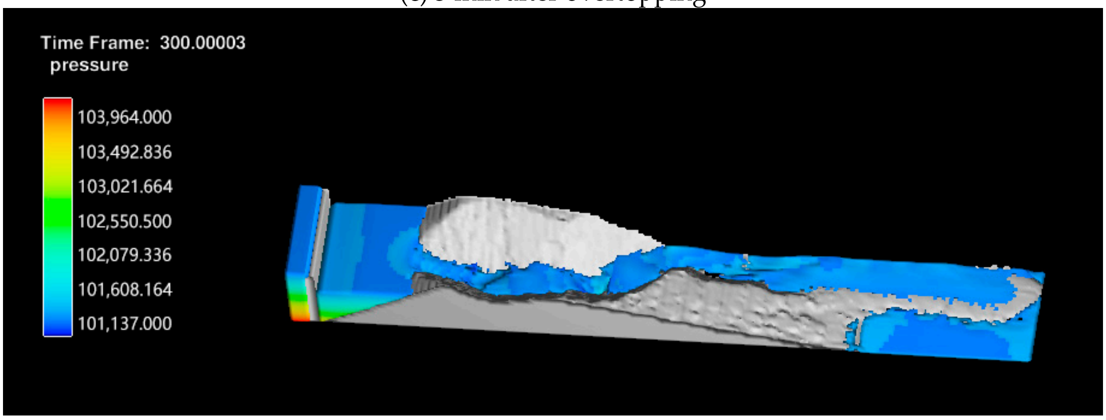

(**d**) 5 min after overtopping

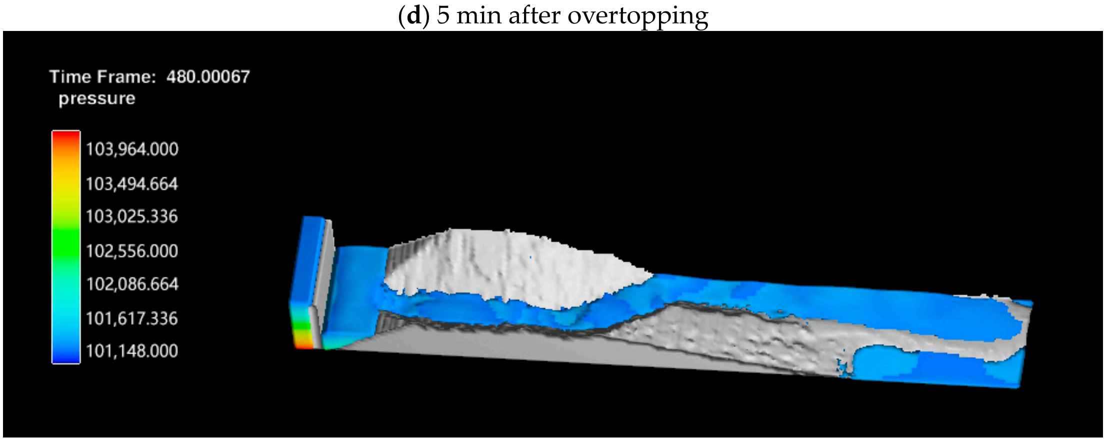

(**e**) 8 min after overtopping

Figure 8. *Cont.*

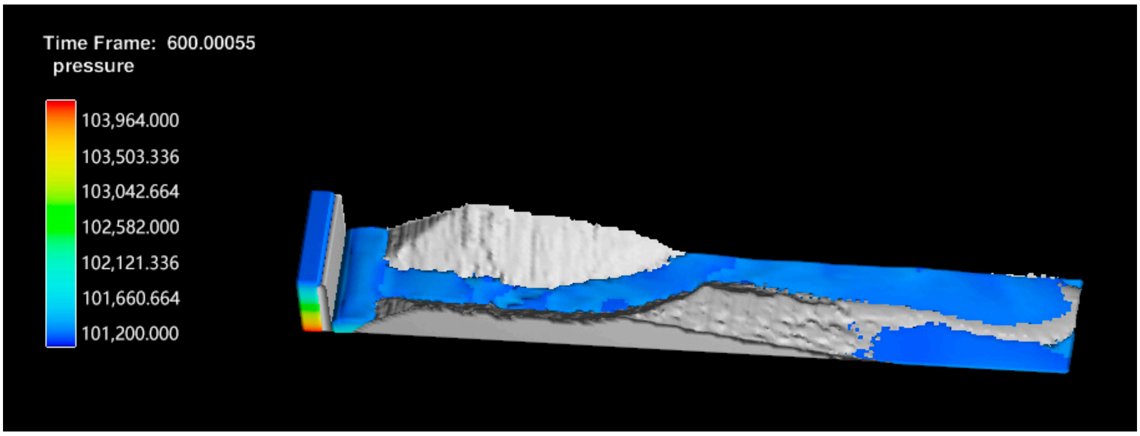

(**f**) 10 min after overtopping

Figure 8. Dam-break process of fly ash mixed with bentonite (4:1) scheme.

5.2. Scheme of Fine Tailings Mixed with 5% Fly Ash

The fine-grained prototype tailings were used as the model dam material for the model test. It can be seen that the development speed of the dam breach and the destruction speed of the dam under the overall hydraulic scouring are obviously faster than the scheme of fly ash mixed with bentonite (4:1) (Figure 9). After 1 min of overtopping, the water flow on the dam crest is relatively uniform, and a Y-shaped scouring surface is formed on the surface of the dam body. The width and depth of the breach develop rapidly at 3~5 min after the overflow, the width of the breach reaches 0.1 m while the depth of the breach reaches 0.2 m. The water flow concentrated on the surface of the dam body forms a connected trench, and the foot of the slope also begins to collapse. At 5 min, the width of the breach is further developed, a large gap appears in the downstream of the dam slope and the dam toe is almost completely damaged. After 8 min of overtopping, the breach at the foot of the slope develops and continues to develop to the top of the dam. After 10 min of overtopping, the breach at the foot and top of the slope become connected, and the dam body is almost completely destroyed. In the whole process, the sediment deposition at the dam toe is less, and the sediment is mainly eroded by entrainment (Figure 10).

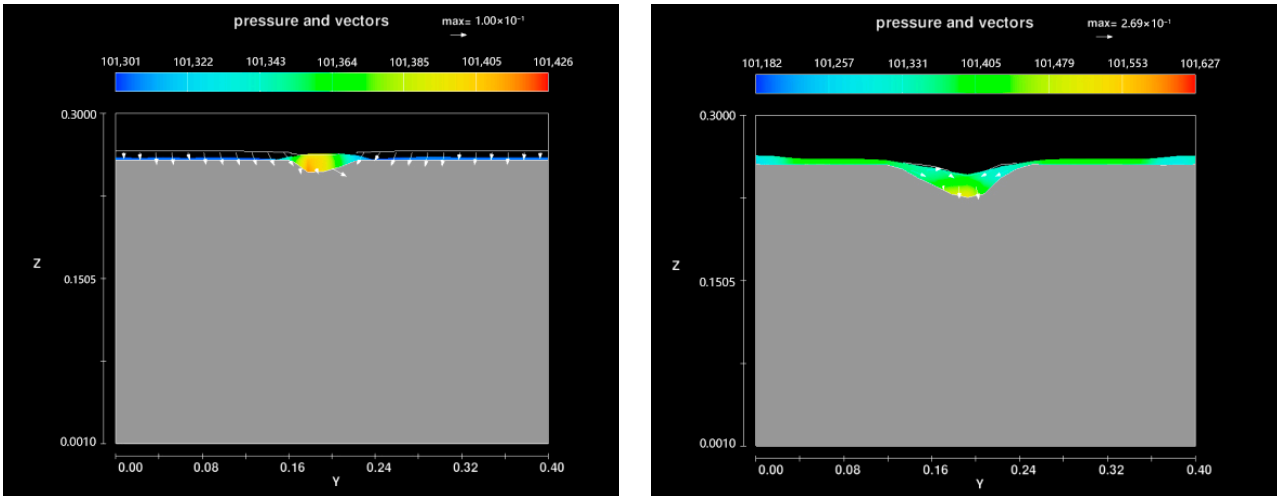

(**a**) Start of overtopping (**b**) 1 min after overtopping

Figure 9. *Cont*.

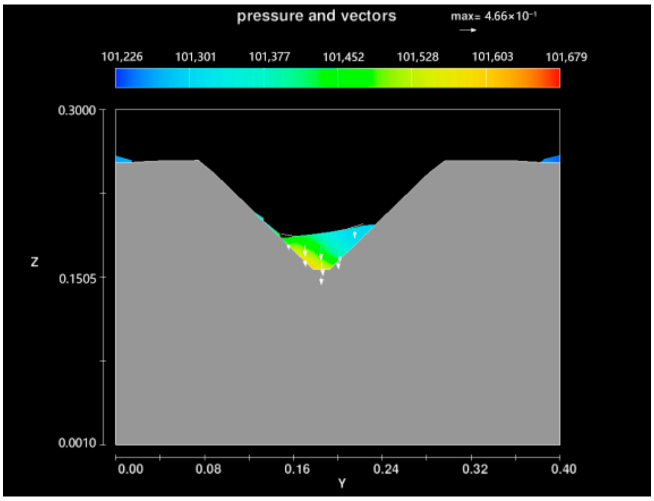

(**c**) 3 min after overtopping

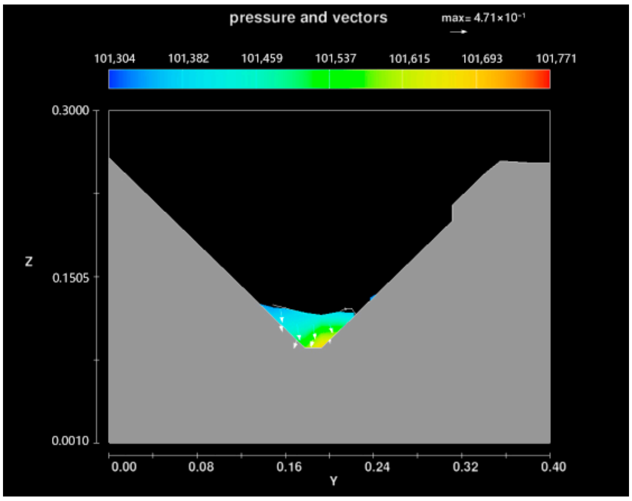

(**d**) 5 min after overtopping

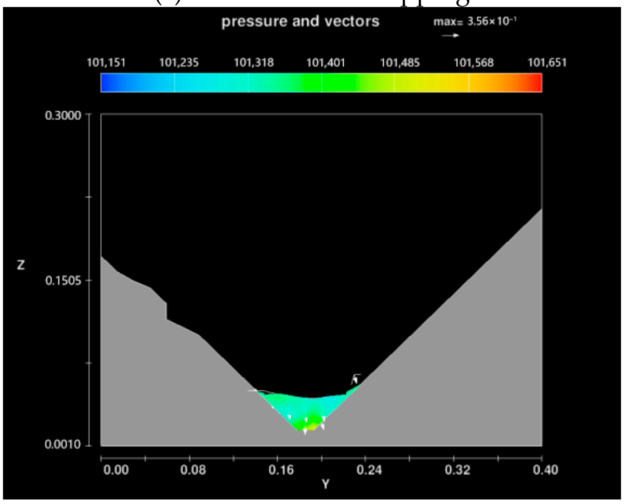

(**e**) 8 min after overtopping

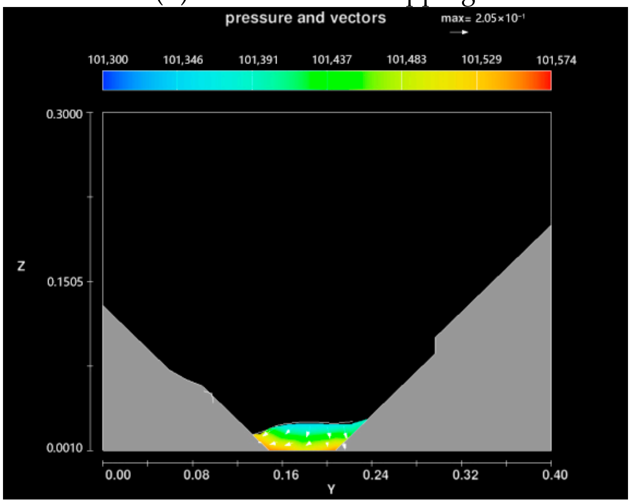

(**f**) 10 min after overtopping

Figure 9. Breach development of fine model sand scheme.

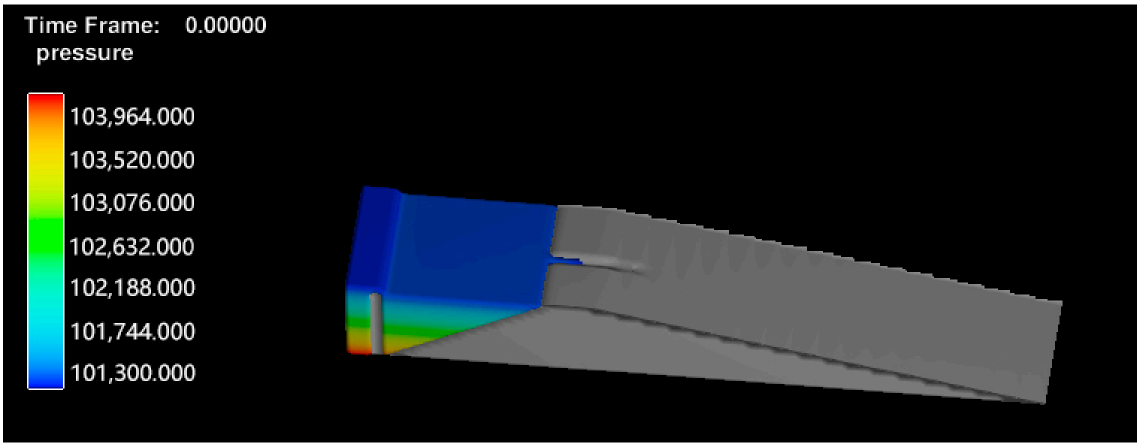

(**a**) Start of overtopping

Figure 10. *Cont.*

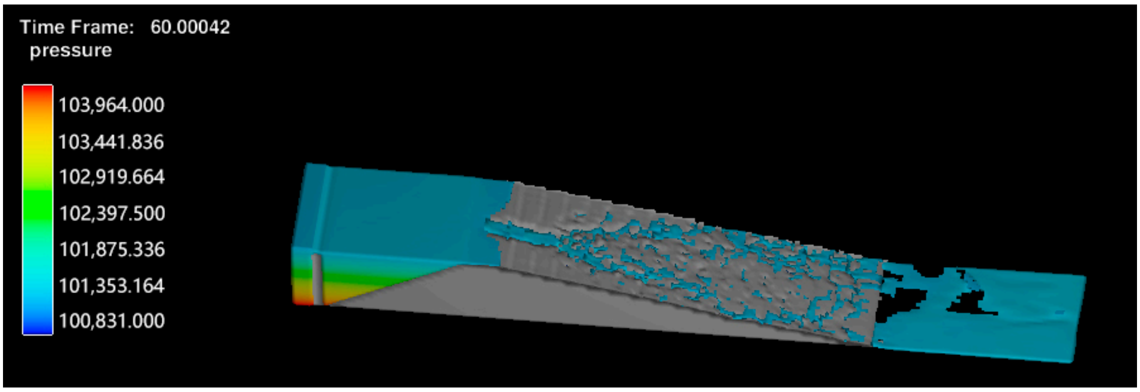

(**b**) 1 min after overtopping

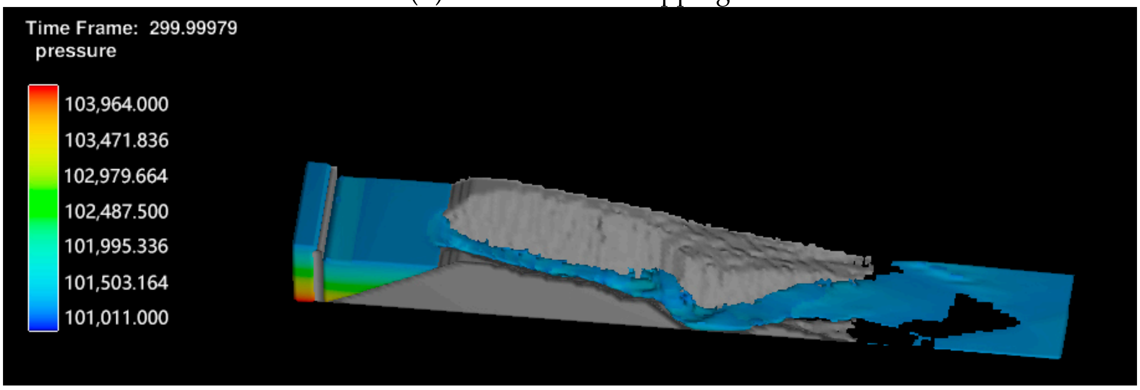

(**c**) 3 min after overtopping

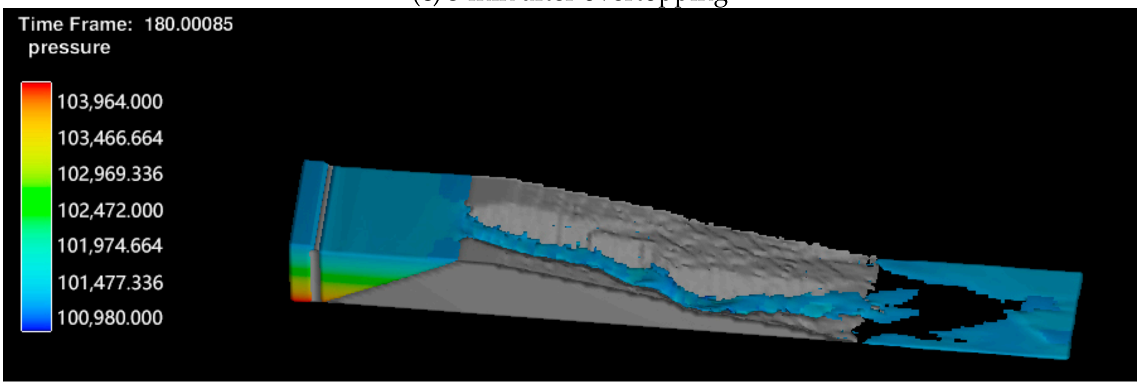

(**d**) 5 min after overtopping

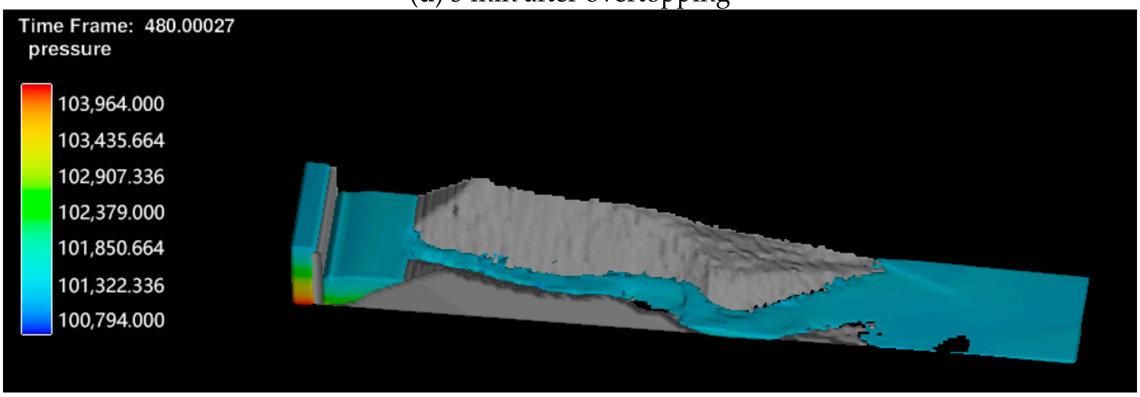

(**e**) 8 min after overtopping

Figure 10. *Cont.*

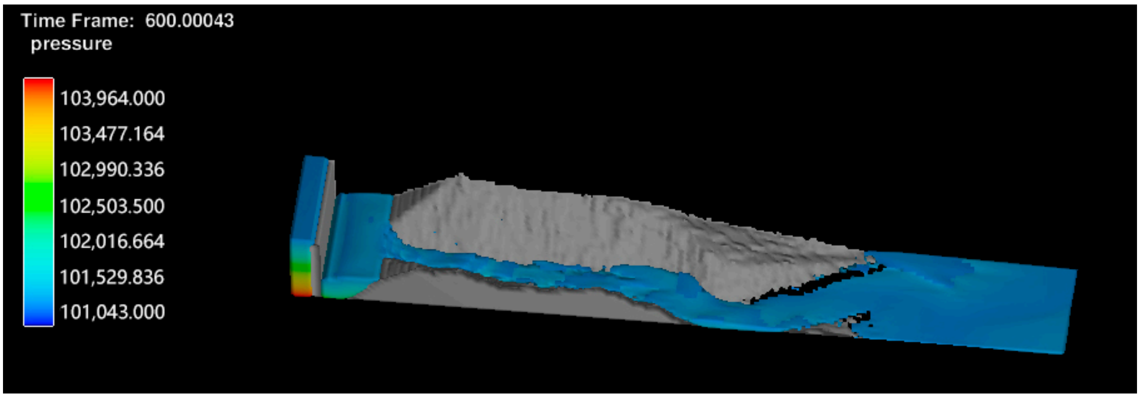

(**f**) 10 min after overtopping

Figure 10. Dam-break process of tailings scheme of fine model.

5.3. Prototype Tailings Scheme

When the prototype sand is used as the model sand in the model test, the development of the breach and the speed of the dam break are obviously slowed down (Figure 11). After 1 min of overtopping, the breach develops slowly and the water flow on the surface of the dam body is relatively uniform. After 3 min of overtopping, the breach developed only 0.15 m and the depth of the breach was only 0.08 m. The water flow scouring groove on the surface of the dam body is initially formed. After 5~8 min of overtopping, the breach develops slowly, a large amount of sediment deposition occurs downstream of the dam slope and the overtopping scouring flow is tortuous, forming a multi-step trapezoidal "scarp". After 15 min of overtopping, the dam body is close to destruction. In terms of overall performance, the erosion speed of the dam body is slow (as shown in Figure 12). Due to the less sediment erosion caused by water entrainment, the sediment movement shows greater shiftability.

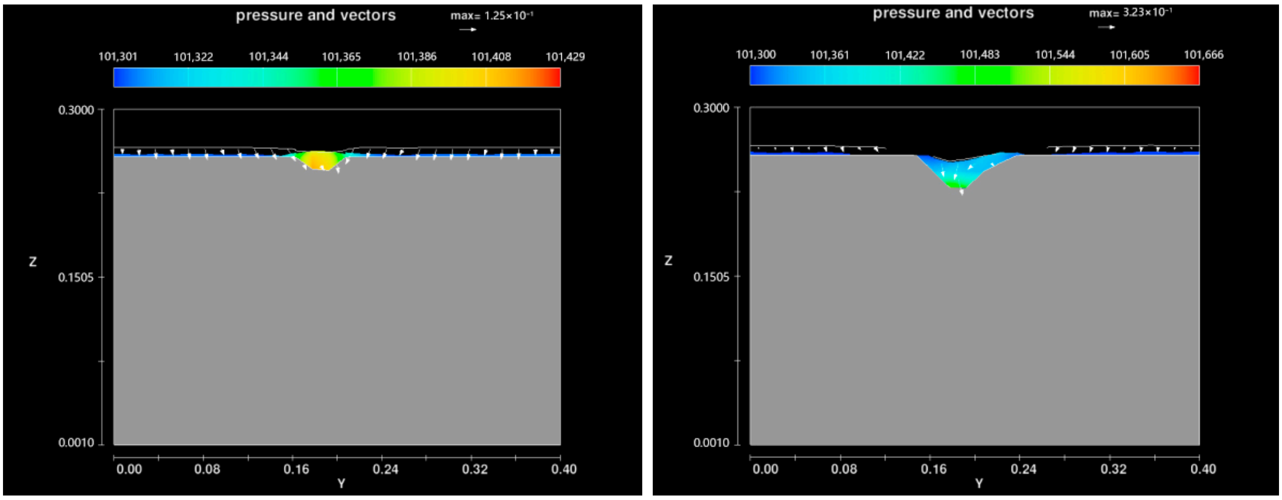

(**a**) Start of overtopping (**b**) 1 min after overtopping

Figure 11. *Cont.*

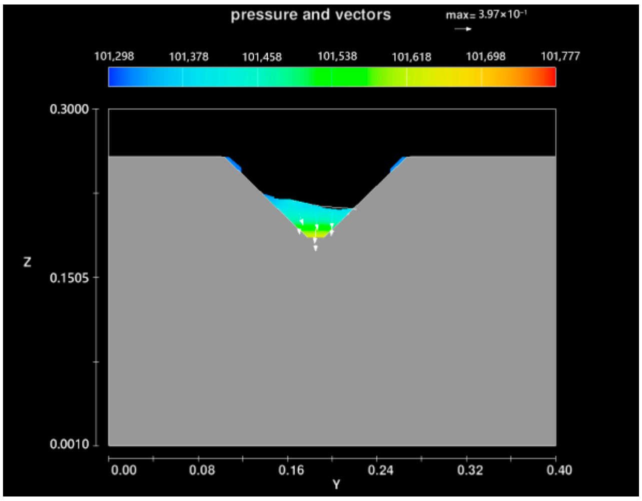

(**c**) 3 min after overtopping

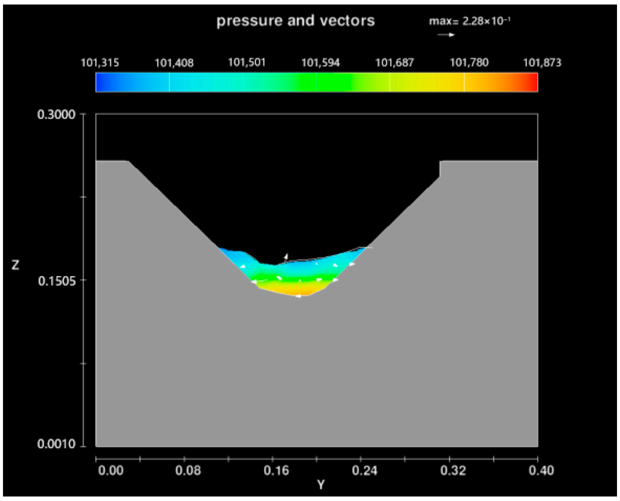

(**d**) 5 min after overtopping

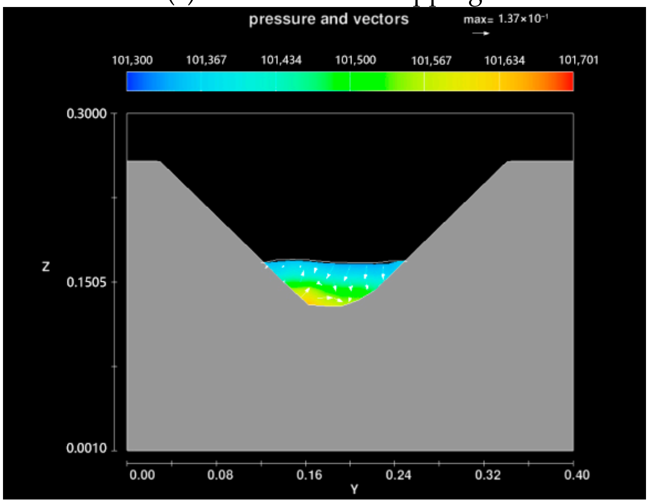

(**e**) 8 min after overtopping

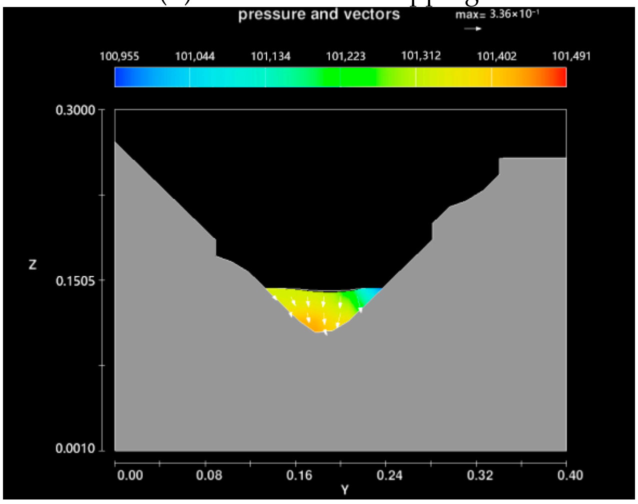

(**f**) 10 min after overtopping

Figure 11. Burst development of model raw sand scheme.

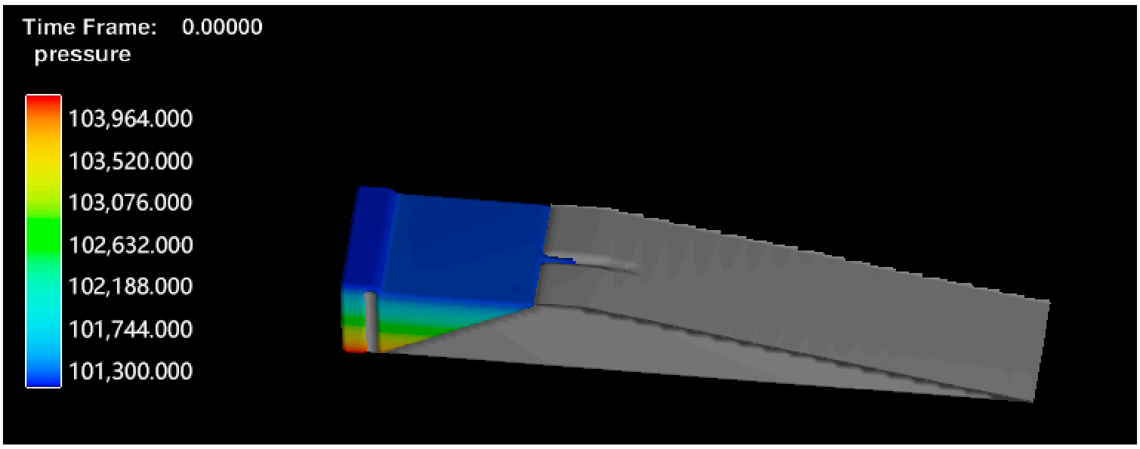

(**a**) Start of overtopping

Figure 12. *Cont.*

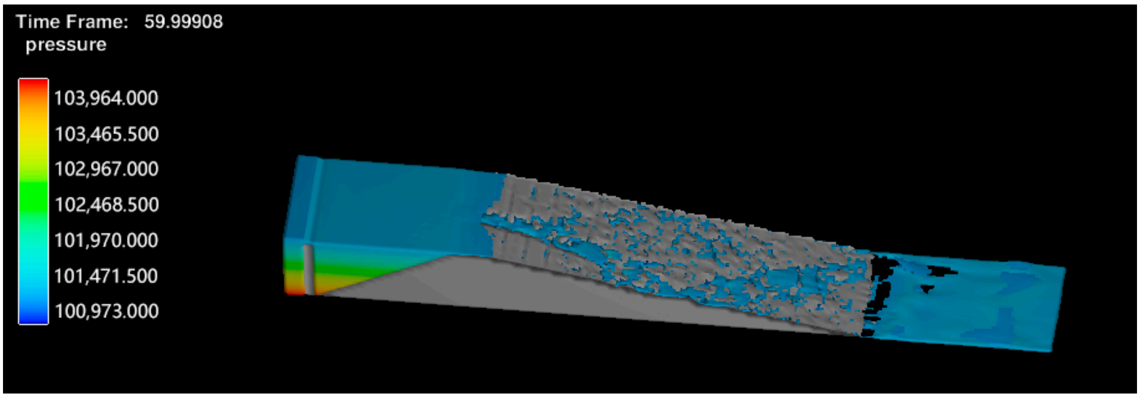

(**b**) 1 min after overtopping

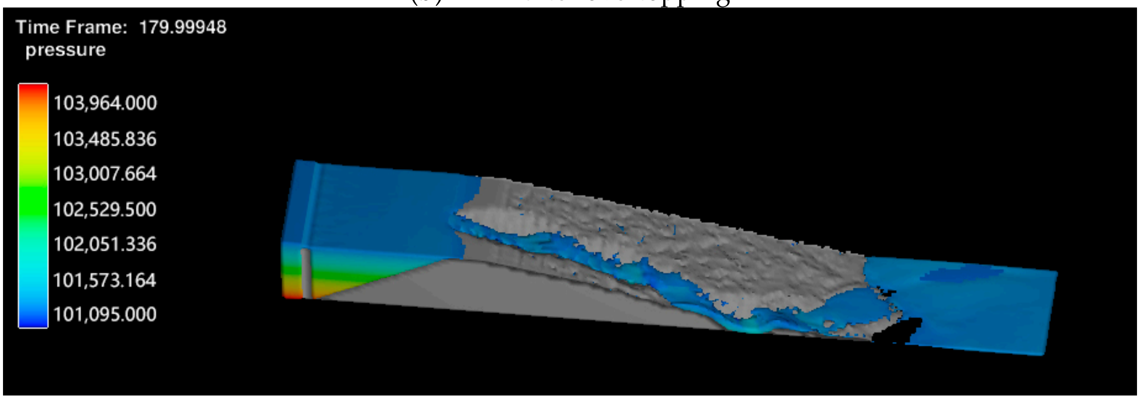

(**c**) 3 min after overtopping

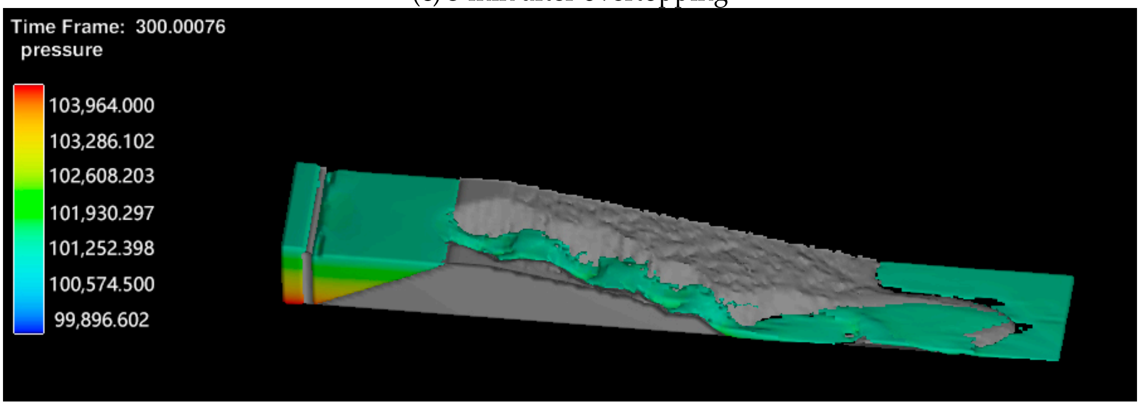

(**d**) 5 min after overtopping

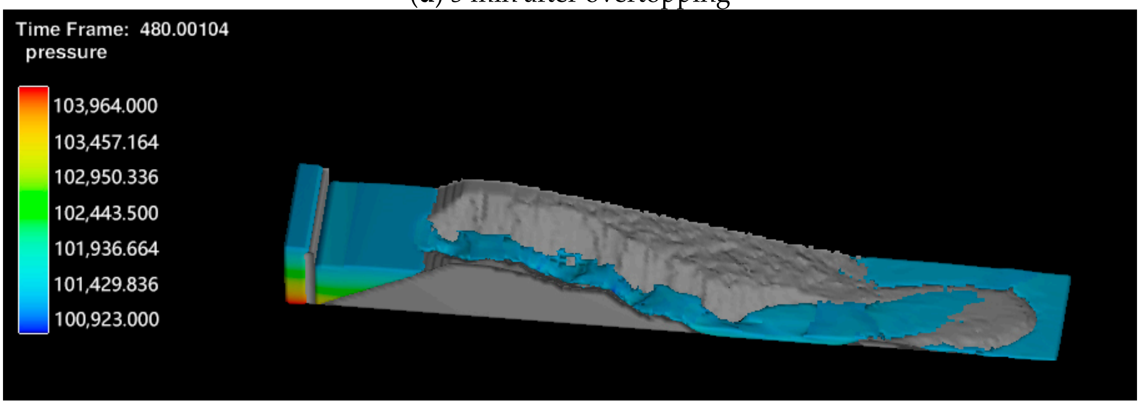

(**e**) 8 min after overtopping

Figure 12. *Cont.*

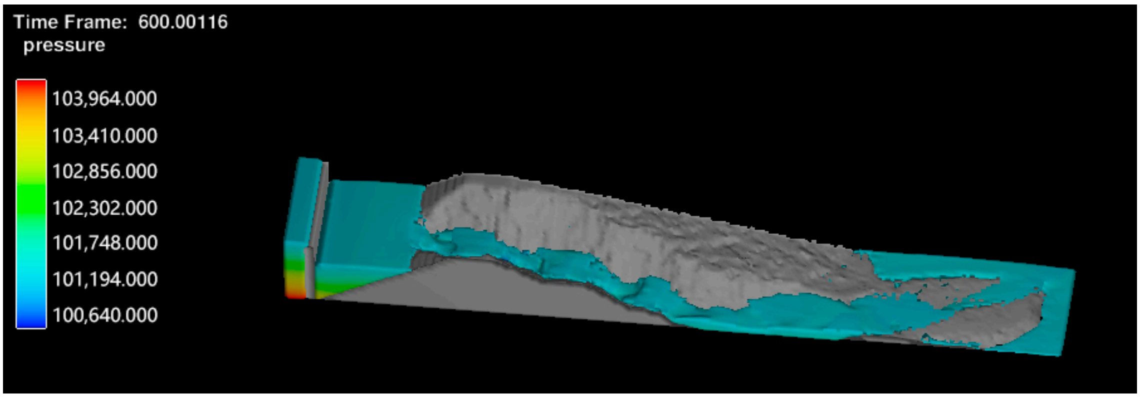

(**f**) 10 min after overtopping

Figure 12. Dam-break process of tailings pond prototype sand scheme.

6. Comparative Analysis and Discussion

According to the overtopping numerical tests of the above three different model schemes, the change law of the model breach width using fine tailings mixed with 5% fly ash is more similar to that of the prototype tailings dam with the breach width reaching the maximum almost at the same time. The breach width of the model using fly ash mixed with bentonite (4:1) increases obviously, and the breach width of this scheme reaches the maximum earlier, which indicates faster erosion. When the prototype tailings are used as the model dam material, the dam-break process shows obvious hysteresis. Even when the time reaches 6000 s, the breach width still does not reach a reasonable size. According to the development law of breach depth, the scheme of fine tailings mixed with 5% fly ash is most similar to the prototype of tailings dam. The breach depth of the scheme of fly ash mixed with bentonite (4:1) shows great fluctuation with the change of time. In the vicinity of 3700 s, it even decreases instead of increasing. Excluding the influence of test contingency, it may be that under the erosion of sediment, the breach deepens, causing the instability and collapse of the slopes on both sides of the breach. This process can reduce the depth of the breach temporarily. The prototype tailings scheme shows more obvious hysteresis of the dam break. In addition, by observing the dam failure characteristics of each scheme, the tailings in the scheme of fly ash mixed with bentonite (4:1) show great mutual displacement, and a large amount of sediment is deposited in the downstream, and the dam failure characteristics are inconsistent with the prototype of the tailings pond. In the prototype tailings scheme, the dam-break speed is obviously slower than that of the prototype tailings pond, and the downstream deposition is larger, which is inconsistent with the prototype tailings pond.

The change law of the breach width and breach depth of the tailings dam with time in the prototype as well as three model schemes is shown in Figure 13. When the breach extends to the dam crest, then the tailings dam is considered to have undergone whole failure. The time interval needed for the tailings dam failure in each scheme can be measured as shown in Table 5. The predicted dam failure time of the model using fine tailings mixed with 5% fly ash is the closest to the dam-break time of the prototype tailings dam, and the dam-break time of the scheme of fly ash mixed with bentonite (4:1) is also relatively close but slightly longer. However, the longest predicted dam failure time by the model scheme using prototype tailings is about 7500 s, which is very different from that of the prototype. Based on the breach process and dam-break time, the reduced model scheme using 5% fly ash mixed with fine tailings can better meet the overtopping failure characteristics of the prototype tailings dam. Above all, the similarity between the overtopping dam-break model and the prototype can be greatly improved by using inception similarity optimization to select the model sand.

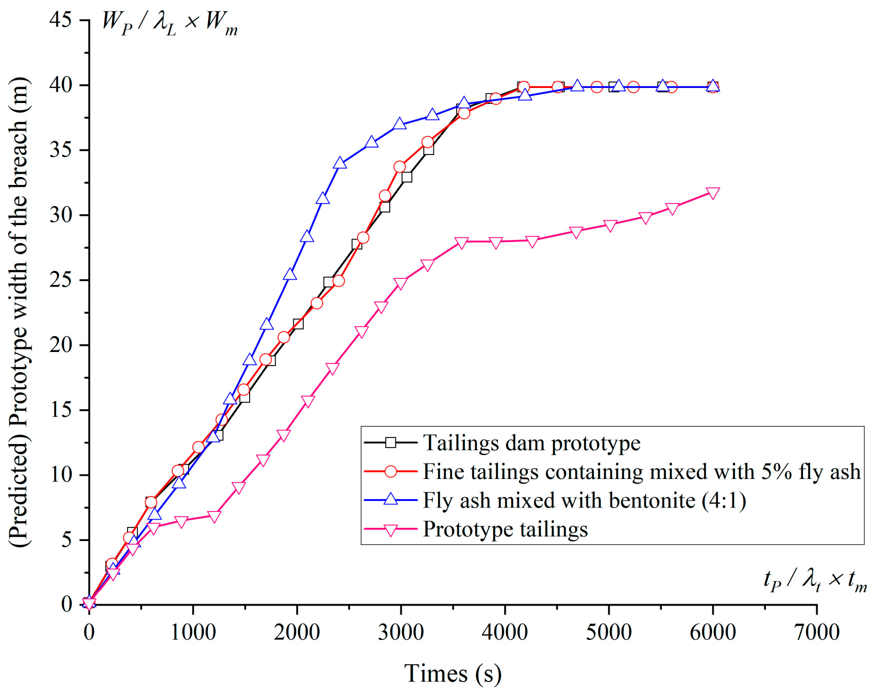

(**a**) Development of breach width

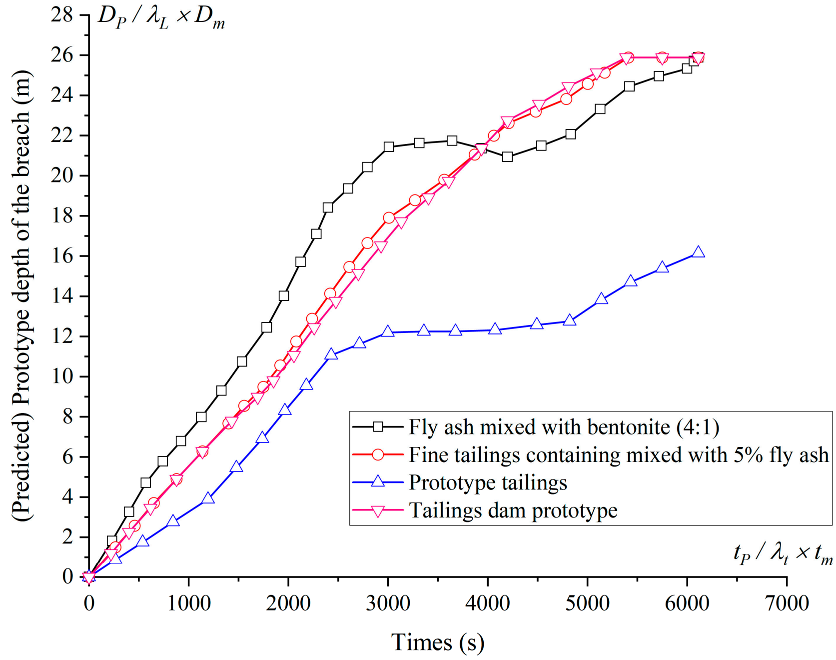

(**b**) Development of breach depth

Figure 13. Comparison of model scheme and tailings dam prototype breakage development characteristics.

Table 5. Comparison of dam-break time.

Name	Fly Ash Mixed with Bentonite (4:1)	Fine Tailings Containing Mixed with 5% Fly Ash	Prototype Tailings	Tailings Dam Prototype
Time (s)	6300	5800	7500	5700

7. Conclusions

Based on the similarity optimization analysis of tailings incipient motion, the overtopping failure process of a prototype tailings dam and reduced-scale model tailings dam is modeled and calculated by using FLOW-3D numerical calculation software, and the development characteristics of tailings dam breach, and the similarity degree between the breach time and the prototype are compared and analyzed under three model sand schemes. The results show that the similarity between the prototype model and the reduced-scale model of overtopping test using tailings is very poor, the model using fly ash mixed with bentonite (4:1) scheme has been greatly improved, and the similarity between the reduced-scale model of fine tailings mixed with fly ash scheme and the prototype model is the best. It is feasible to compare and select the model materials of tailings dam failure due to overtopping by using the method of inception similarity optimization.

Author Contributions: Conceptualization, D.Q. and H.L.; methodology, D.Q. and H.L.; software, J.X.; validation, D.Q. and H.L.; formal analysis, D.Q. and J.X.; investigation, D.Q. and J.X.; writing—original draft preparation, D.Q. and J.X.; writing—review and editing, H.L.; supervision, H.L.; funding acquisition, H.L. All authors have read and agreed to the published version of the manuscript.

Funding: This research was funded by the National Natural Science Foundation of China (grant number 42062018) and the National Natural Science Foundation of Jiangxi Province (grant number 20224BAB203039).

Institutional Review Board Statement: Not applicable.

Informed Consent Statement: Not applicable.

Data Availability Statement: The original contributions presented in the study are included in the article, further inquiries can be directed to the corresponding author.

Conflicts of Interest: Author Deli Qiu was employed by the company Jiangxi Provincial Architectural Design and Research Institute Group Co., Ltd. The remaining authors declare that the research was conducted in the absence of any commercial or financial relationships that could be construed as a potential conflict of interest.

References

1. Grebby, S.; Sowter, A.; Gluyas, J.; Toll, D.; Gee, D.; Athab, A.; Girindran, R. Advanced analysis of satellite data reveals ground deformation precursors to the Brumadinho Tailings Dam collapse. *Commun. Earth Environ.* **2021**, *2*, 2. [CrossRef]
2. Jin, J.; Song, C.; Liang, B.; Chen, Y.; Su, M. Dynamic characteristics of tailings reservoir under seismic load. *Environ. Earth Sci.* **2018**, *77*, 654. [CrossRef]
3. Piciullo, L.; Storrsten, E.B.; Liu, Z.; Farrokh, N.; Lacasse, S. A new look at the statistics of tailings dam failures. *Eng. Geol.* **2022**, *303*, 106657. [CrossRef]
4. Rico, M.; Benito, G.; Salgueiro, A.R.; Diez-Herrero, A.; Pereira, H.G. A review of the European incidents in the worldwide context. *J. Hazard. Mater.* **2008**, *152*, 846–852. [CrossRef] [PubMed]
5. Silva, R.L.H.; Alcantara, E.; Park, E.; Negri, R.G.; Lin, Y.N.; Bernardo, N.; Mendes, T.S.G.; Souza, F.C.R. The 2019 Brumadinho tailings dam collapse: Possible cause and impacts of the worst human and environmental disaster in Brazil. *Int. J. Appl. Earth Observ. Geoinf.* **2020**, *90*, 102119. [CrossRef]
6. Amini, M.; Ardestani, A.; Khosravi, M.H. Stability analysis of slide-toe-toppling failure. *Eng. Geol.* **2017**, *228*, 82–96. [CrossRef]
7. Wang, L.N.; Lian, Y.Q.; Li, Z. Hydraulic analysis for strategic management of flood risks along the Illinois River. *Environ. Earth Sci.* **2019**, *78*, 80. [CrossRef]
8. Wei, Z.A.; Yin, G.Z.; Wan, L.; Li, G.Z. A case study on a geotechnical investigation of drainage methods for heightening a tailings dam. *Environ. Earth Sci.* **2016**, *75*, 106. [CrossRef]
9. Jiang, X.; Xu, W.; Chen, X.; Chen, H.; Zhang, C. Experiments on the characteristics of breach variation-s due to natural dam overtopping. *Environ. Earth Sci.* **2021**, *80*, 373. [CrossRef]
10. Tao, Z.; Zhu, C.; He, M.; Karakus, M. A physical modeling-based study on the control mechanisms of negative Poisson's ratio anchor cable on the stratifed toppling deformation of anti-inclined slopes. *Int. J. Rock. Mech. Min. Sci.* **2021**, *138*, 104632. [CrossRef]
11. Zhou, G.G.D.; Li, S.; Lu, X.Q.; Tang, H. Large-scale landslide dam breach experiments: Overtopping and "overtopping and seepage" failures. *Eng. Geol.* **2022**, *304*, 106680. [CrossRef]
12. Dazzi, S.; Vacondio, R.; Mignosa, P.; Aureli, F. Assessment of presimulated scenarios as a non-structural measure for food management in case of levee-breach inundations. *Int. J. Disaster Risk Reduct.* **2022**, *74*, 102926. [CrossRef]

13. Zhang, J.Y.; Fan, G.; Li, H.B.; Zhou, J.W.; Yang, X.G. Large-scale feld model tests of landslide dam breaching. *Eng. Geol.* **2021**, *293*, 106322. [CrossRef]
14. Crouzy, B.; Perona, P. Biomass selection by foods and related timescales. Part 2: Stochastic modeling. *Adv. Water Resour.* **2012**, *39*, 97–105. [CrossRef]
15. Jin, J.; Song, C.; Chen, Y. Investigation of a fluid–solid coupling model for a tailings dam with infiltration of suspended particles. *Environ. Earth Sci.* **2017**, *76*, 758. [CrossRef]
16. Robert, E.T.; Matthew, F.J.; Lynne, E.F.; Daniel, R.P.; Tjeerd, J.B.; Jasper, T.D.; Michalis, I.V. Physical modelling of water, fauna and fora: Knowledge gaps, avenues for future research and infrastructural needs. *J. Hydraul. Res.* **2014**, *52*, 311–325. [CrossRef]
17. Altaee, A.; Fellenius, B.H. Physical modeling in sand. *Can. Geotech. J.* **1994**, *31*, 420–431. [CrossRef]
18. Lin, H.; Luo, J.; Zhou, C.; Tao, Z. Research on model material selection based on inception similarity in impact analysis of flood overtopping on tailings dam. *Environ. Earth Sci.* **2023**, *82*, 276. [CrossRef]
19. Aussillous, P.; Chauchat, J.; Pailha, M.; Medale, M.; Guazzelli, E. Investigation of the mobile granular layer in bedload transport by laminar shearing fows. *J. Fluid. Mech.* **2013**, *736*, 594–615. [CrossRef]
20. Chiodi, F.; Claudin, P.; Andreotti, B. A two-phase fow model of sediment transport: Transition from bedload to suspended load. *J. Fluid. Mech.* **2014**, *755*, 561–581. [CrossRef]
21. Middleton, G.V.; Southard, J.B. *Mechanics of Sediment Movement*; SEPM Soc Sedim Geol: Claremont, CA, USA, 1984; Volume 3. [CrossRef]
22. Shields, A. *Application of Similarity Principles and Turbulence Research to Bed-Load Movement Report*; California Institute of Technology: Pasadena, CA, USA, 1936; Available online: https://repository.tudelft.nl/islandora/object/uuid:a66ea380-ffa3-449b-b59f-38a35b2c6658 (accessed on 28 November 2023).
23. Farinella, G.M.; Battiato, S.; Cipolla, R. *Advanced Topics in Computer Vision*; Springer Publishing Company, Incorporated: New York, NY, USA, 2013; Available online: https://dl.acm.org/doi/book/10.5555/2541784 (accessed on 28 November 2023).
24. *ASTM D6913/D6913M-17*; Standard Test Methods for Particle-Size Distribution (Gradation) of Soils Using Sieve Analysis. ASTM International: West Conshohkchen, PA, USA, 2017.
25. *ASTM D854/D864-23*; Standard Test Methods for Specific Gravity of Soil Solids by the Water Displacement Method. ASTM International: West Conshohkchen, PA, USA, 2023.